

Research Article

Research on Dynamic Load Identification Based on Explicit Wilson- θ and Improved Regularization Algorithm

Yuchuan Fan , Chunyu Zhao , and Hongye Yu 

School of Mechanical Engineering and Automation, Northeastern University, Shenyang 110819, China

Correspondence should be addressed to Chunyu Zhao; chyzhao@mail.neu.edu.cn

Received 8 November 2018; Revised 23 January 2019; Accepted 28 January 2019; Published 25 March 2019

Academic Editor: Nerio Tullini

Copyright © 2019 Yuchuan Fan et al. This is an open access article distributed under the Creative Commons Attribution License, which permits unrestricted use, distribution, and reproduction in any medium, provided the original work is properly cited.

In the research of dynamic load identification, the method of obtaining kernel function matrix is usually rather cumbersome. To solve this problem, an explicit dynamic load identification algorithm based on the Wilson- θ (DLIAEW) method is proposed to easily obtain the kernel function matrix as long as the parameters of the system are known. To aim at the ill-posed problem in the inverse problem, this paper improves the Tikhonov regularization, proposes an improved regularization algorithm (IRA), and introduces the U-curve method to determine the regularization parameters. In the numeric simulation investigation of a four dofs vibrating system, effects of the sampling frequency and the noise level on the regularization parameters and the identification errors of impact and harmonic loads for the IRA are discussed in comparison with the Tikhonov regularization. Finally, the experiments of a cantilever beam excited by impact and harmonic loads are carried out to verify the advantages of the IRA.

1. Introduction

Load identification plays an important role in many engineering studies, such as reliability analysis, fault diagnosis, and health monitoring of mechanical power structures [1, 2]. Dynamic load identification methods include the frequency-domain method and the time-domain method [3]. Compared with the time-domain method, the study of dynamic load identification in the frequency domain starts earlier, and the theory is more mature. The frequency-domain method determines the dynamic force spectrum according to the relation between the transfer function matrix and the response spectrum of the system, or calculates the dynamic characteristics of the modal force in the frequency domain after the modal coordinate transformation [4]. The time-domain method is the inverse analysis based on the complex convolution relation between the load and the response, and the temporal history of dynamic loads is retrieved directly in the time domain. The time-domain method does not need Fourier transform, the result is intuitionistic, and the research of the time-domain method in recent years also has a great development.

Dynamic load identification belongs to an ill-posedness of the inverse problem, which will lead to not useful solutions

which cause large deviations from the exact solutions because of measured noise data and the randomness of structural parameters [5, 6]. In recent years, much effort on solving this ill-posed problem has been devoted to overcoming the effects of structural uncertainty and measurement noise and improving the accuracy of dynamic load identification. The effects of matrix ill-conditioning were overcome by using methods such as pseudoinversion of overdetermined matrices, singular value rejection, singular value decomposition (SVD), and regularization techniques. Through both simulation and experiment on a flat rectangular plate, Thite and Thompson [7–9] proposed an assessment which was made of the success and failure of various strategies for dealing with the problems of ill-conditioning, in particular overdetermination and singular value rejection. Inoue et al. [10] utilized the SVD to locate the small singular values which were eliminated in computation of the frequency response function. Inoue et al. [11], Jacquelin et al. [12], and Adams and Doyle [13] described more systematic approaches of the SVD to solve the reconstruction problems of harmonic and nonharmonic forces.

Using shape function to approximate dynamic load, kernel function response, and measured structure response, Liu et al. [14] established a time-domain dynamic Galerkin

method (TDGM) to improve the accuracy of the identified dynamic load by taking shape function as the weighting function. Furthermore, they also proposed an efficient interpolation-based method to reduce ill-posedness by discretizing the load history into a series of time elements approximated through interpolation functions [15]. Qiao et al. [16–20] proposed the cubic B-spline collocation method and the sparse deconvolution method to identify impact loads. Through reconstructing the dynamic loads in the deterministic structure of the thin-walled cylindrical shell and airfoil structure, Wang et al. [21] developed a fast convergent iteration regularization method for identifying dynamic loads. The above works all focused on deterministic structures. However, practical structures have usually some random parameters. Hence, unknown load identified by virtue of a deterministic model describing a stochastic one would not be accurate. Expressing dynamic loads as the functions of time and random parameters in the time domain by Liu et al. [22, 23] transformed the dynamic models of uncertain structures into equivalent deterministic equations to identify unknown loads.

In order to solve ill-posed problem for load identification, the choice of regularization parameters plays a key role in regularization, and there are many methods to select regularization parameters, such as the L-curve method, the generalized cross validation (GCV), the U-curve method, and the discrepancy principle [24–27]. To mitigate error propagation and ill-posed problem during the process of identification, Jia et al. [28, 29] proposed a weighted regularization approach based on the proper orthogonal decomposition (POD), in which the regularization parameter was selected by the GCV method.

In this paper, an improved regulation algorithm is proposed to solve the ill-posed problem of dynamic load identification. In the next section, the explicit form of Wilson- θ is deduced, and a load identification algorithm based on the explicit Wilson- θ method is proposed. In Section 3, the IRA is proposed, and the U-curve method is introduced to select regularization parameters. The numeric simulations of a four dofs vibrating system and the experiments of a cantilever beam are conducted to verify the load identification effectiveness of the IRA in Sections 4 and 5, respectively. Finally, conclusions are given in Section 6.

2. Dynamic Load Identification Algorithm Based on Explicit Wilson- θ Method

The dynamic equation of a damped linear system with multiple dofs is

$$\mathbf{M}\ddot{\mathbf{x}} + \mathbf{C}\dot{\mathbf{x}} + \mathbf{K}\mathbf{x} = \mathbf{P}, \quad (1)$$

where \mathbf{M} denotes the mass matrix, \mathbf{C} denotes the damping matrix and \mathbf{K} denotes the stiffness matrix. \mathbf{P} is the load vector acting on the structure. $\ddot{\mathbf{x}}$, $\dot{\mathbf{x}}$, and \mathbf{x} denote the acceleration vectors, the velocity vectors, and the displacement vectors, respectively. Assuming that the structure is expressed as Rayleigh damping, it is expressed as

$$\mathbf{C} = \alpha_1 \mathbf{M} + \alpha_2 \mathbf{K}, \quad (2)$$

where α_1 and α_2 are the constants selected to achieve the desired damping ratio at two preselected periods/frequencies. The damping ratio for the n th mode of vibration is then given by [30]

$$\zeta_n = \frac{\alpha_1}{2\omega_n} + \frac{\omega_n}{2}\alpha_2, \quad (3)$$

where ω_n corresponds to the circular frequency of the n th mode.

In practical application, it is difficult to obtain the closed-form analytical solution of Equation (1) because of the complexity of structure and excitation. The dynamic equation is usually solved directly by a numerical integration method with the time-step method.

The Wilson- θ method assumes that the acceleration varies linearly within the time interval $[t, t + \theta\Delta t]$ ($\theta \geq 1$), as shown in Figure 1. In linear problems, the method is unconditionally stable for $\theta \geq 1.37$, so $\theta = 1.4$ is usually employed [31].

Let δ be a time variable starting at time t , which is applicable to $0 \leq \delta \leq \theta\Delta t$. According to the assumption of linear acceleration, the acceleration in this range can be expressed as follows:

$$\ddot{\mathbf{x}}_{t+\delta} = \ddot{\mathbf{x}}_t + \frac{\delta}{\theta\Delta t} (\ddot{\mathbf{x}}_{t+\theta\Delta t} - \ddot{\mathbf{x}}_t). \quad (4)$$

Integrating equation (4) once and twice, respectively, one can get

$$\dot{\mathbf{x}}_{t+\delta} = \dot{\mathbf{x}}_t + \ddot{\mathbf{x}}_t \delta + \frac{\delta^2}{2\theta\Delta t} (\ddot{\mathbf{x}}_{t+\theta\Delta t} - \ddot{\mathbf{x}}_t), \quad (5)$$

$$\mathbf{x}_{t+\delta} = \mathbf{x}_t + \dot{\mathbf{x}}_t \delta + \frac{1}{2}\ddot{\mathbf{x}}_t \delta^2 + \frac{\delta^3}{6\theta\Delta t} (\ddot{\mathbf{x}}_{t+\theta\Delta t} - \ddot{\mathbf{x}}_t). \quad (6)$$

Inserting $\delta = \theta\Delta t$ into equations (5) and (6), we get

$$\dot{\mathbf{x}}_{t+\theta\Delta t} = \dot{\mathbf{x}}_t + \frac{\theta\Delta t}{2} (\ddot{\mathbf{x}}_{t+\theta\Delta t} + \ddot{\mathbf{x}}_t), \quad (7)$$

$$\mathbf{x}_{t+\theta\Delta t} = \mathbf{x}_t + \theta\Delta t \dot{\mathbf{x}}_t + \frac{\theta^2 \Delta t^2}{6} (\ddot{\mathbf{x}}_{t+\theta\Delta t} + 2\ddot{\mathbf{x}}_t). \quad (8)$$

According to equations (7) and (8), the acceleration and velocity of $t + \theta\Delta t$ can be expressed by displacement:

$$\ddot{\mathbf{x}}_{t+\theta\Delta t} = \frac{6}{\theta^2 \Delta t^2} (\mathbf{x}_{t+\theta\Delta t} - \mathbf{x}_t) - \frac{6}{\theta\Delta t} \dot{\mathbf{x}}_t - 2\ddot{\mathbf{x}}_t, \quad (9)$$

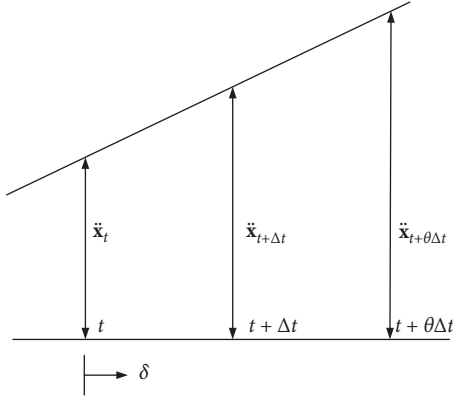
$$\dot{\mathbf{x}}_{t+\theta\Delta t} = \frac{3}{\theta\Delta t} (\mathbf{x}_{t+\theta\Delta t} - \mathbf{x}_t) - 2\dot{\mathbf{x}}_t - \frac{\theta\Delta t}{2} \ddot{\mathbf{x}}_t. \quad (10)$$

Then, the dynamic equation at $t + \theta\Delta t$ can be expressed as follows:

$$\mathbf{M}\ddot{\mathbf{x}}_{t+\theta\Delta t} + \mathbf{C}\dot{\mathbf{x}}_{t+\theta\Delta t} + \mathbf{K}\mathbf{x}_{t+\theta\Delta t} = \mathbf{P}_{t+\theta\Delta t}, \quad (11)$$

with

$$\mathbf{P}_{t+\theta\Delta t} = \mathbf{P}_t + \theta(\mathbf{P}_{t+\Delta t} - \mathbf{P}_t). \quad (12)$$

FIGURE 1: Model of the Wilson- θ method.

Inserting equations (9), (10), and (12) into (11) yields

$$\mathbf{x}_{t+\theta\Delta t} = \widehat{\mathbf{K}}^{-1} \widehat{\mathbf{P}}_{t+\theta\Delta t}, \quad (13)$$

with

$$\widehat{\mathbf{K}} = \mathbf{K} + \frac{3}{\theta\Delta t} \mathbf{C} + \frac{6}{\theta^2\Delta t^2} \mathbf{M}, \quad (14)$$

$$\begin{aligned} \widehat{\mathbf{P}}_{t+\theta\Delta t} = & \mathbf{P}_t + \theta(\mathbf{P}_{t+\Delta t} - \mathbf{P}_t) + \mathbf{M} \left(\frac{6}{\theta^2\Delta t^2} \mathbf{x}_t + \frac{6}{\theta\Delta t} \dot{\mathbf{x}}_t + 2\ddot{\mathbf{x}}_t \right) \\ & + \mathbf{C} \left(\frac{3}{\theta\Delta t} \mathbf{x}_t + 2\dot{\mathbf{x}}_t + \frac{\theta\Delta t}{2} \ddot{\mathbf{x}}_t \right). \end{aligned} \quad (15)$$

Solving equation (13) for $\mathbf{x}_{t+\theta\Delta t}$ and then inserting $\mathbf{x}_{t+\theta\Delta t}$ into equation (9) yields $\ddot{\mathbf{x}}_{t+\theta\Delta t}$. Substituting equation (9) into (4) and taking $\delta = \Delta t$, we obtain

$$\ddot{\mathbf{x}}_{t+\Delta t} = \frac{6}{\theta^3\Delta t^2} (\mathbf{x}_{t+\theta\Delta t} - \mathbf{x}_t) - \frac{6}{\theta^2\Delta t} \dot{\mathbf{x}}_t + \left(1 - \frac{3}{\theta}\right) \ddot{\mathbf{x}}_t. \quad (16)$$

Substituting equation (4) into (5) and (6) and taking $\delta = \Delta t$, we get

$$\dot{\mathbf{x}}_{t+\Delta t} = \dot{\mathbf{x}}_t + \frac{\Delta t}{2} (\ddot{\mathbf{x}}_{t+\Delta t} + \ddot{\mathbf{x}}_t), \quad (17)$$

$$\mathbf{x}_{t+\Delta t} = \mathbf{x}_t + \Delta t \dot{\mathbf{x}}_t + \frac{\Delta t^2}{6} (\ddot{\mathbf{x}}_{t+\Delta t} + 2\ddot{\mathbf{x}}_t). \quad (18)$$

Inserting equations (14) and (15) into (13) yields

$$\begin{aligned} \mathbf{x}_{t+\theta\Delta t} = & \widehat{\mathbf{K}}^{-1} (1 - \theta) \mathbf{P}_t + \theta \widehat{\mathbf{K}}^{-1} \mathbf{P}_{t+\Delta t} \\ & + \left(\frac{6}{\theta^2\Delta t^2} \mathbf{M} \widehat{\mathbf{K}}^{-1} + \frac{3}{\theta\Delta t} \mathbf{C} \widehat{\mathbf{K}}^{-1} \right) \mathbf{x}_t \\ & + \left(\frac{6}{\theta\Delta t} \mathbf{M} \widehat{\mathbf{K}}^{-1} + 2\mathbf{C} \widehat{\mathbf{K}}^{-1} \right) \dot{\mathbf{x}}_t \\ & + \left(2\mathbf{M} \widehat{\mathbf{K}}^{-1} + \frac{\theta\Delta t}{2} \mathbf{C} \widehat{\mathbf{K}}^{-1} \right) \ddot{\mathbf{x}}_t. \end{aligned} \quad (19)$$

Substituting equation (19) into (16) and considering $\mathbf{I} = \widehat{\mathbf{K}}^{-1} \widehat{\mathbf{K}}$, we obtain

$$\ddot{\mathbf{x}}_{t+\Delta t} = \mathbf{C}_0 \mathbf{P}_t + \mathbf{C}_1 \mathbf{P}_{t+\Delta t} + \mathbf{C}_d \mathbf{x}_t + \mathbf{C}_v \dot{\mathbf{x}}_t + \mathbf{C}_a \ddot{\mathbf{x}}_t, \quad (20)$$

with

$$\begin{aligned} \mathbf{C}_0 &= \frac{6}{\theta^3\Delta t^2} \widehat{\mathbf{K}}^{-1} (1 - \theta), \\ \mathbf{C}_1 &= \frac{6}{\theta^2\Delta t^2} \widehat{\mathbf{K}}^{-1}, \\ \mathbf{C}_d &= \frac{-6}{\theta^3\Delta t^2} \widehat{\mathbf{K}}^{-1} \mathbf{K}, \\ \mathbf{C}_v &= \frac{6}{\theta^2\Delta t} \left(\frac{6}{\theta^2\Delta t^2} \mathbf{M} \widehat{\mathbf{K}}^{-1} + \frac{2}{\theta\Delta t} \mathbf{C} \widehat{\mathbf{K}}^{-1} - \mathbf{I} \right), \\ \mathbf{C}_a &= \frac{12}{\theta^3\Delta t^2} \mathbf{M} \widehat{\mathbf{K}}^{-1} + \frac{3}{\theta^2\Delta t} \mathbf{C} \widehat{\mathbf{K}}^{-1} + \left(1 - \frac{3}{\theta}\right) \mathbf{I}. \end{aligned} \quad (21)$$

Inserting equation (20) into (17) yields

$$\dot{\mathbf{x}}_{t+\Delta t} = \mathbf{B}_0 \mathbf{P}_t + \mathbf{B}_1 \mathbf{P}_{t+\Delta t} + \mathbf{B}_d \mathbf{x}_t + \mathbf{B}_v \dot{\mathbf{x}}_t + \mathbf{B}_a \ddot{\mathbf{x}}_t, \quad (22)$$

with

$$\begin{aligned} \mathbf{B}_0 &= \frac{\Delta t}{2} \mathbf{C}_0, \\ \mathbf{B}_1 &= \frac{\Delta t}{2} \mathbf{C}_1, \\ \mathbf{B}_d &= \frac{\Delta t}{2} \mathbf{C}_d, \\ \mathbf{B}_v &= \frac{\Delta t}{2} \mathbf{C}_v + \mathbf{I}, \\ \mathbf{B}_a &= \frac{\Delta t}{2} (\mathbf{C}_a + \mathbf{I}). \end{aligned} \quad (23)$$

Inserting equation (20) into (18) yields

$$\mathbf{x}_{t+\Delta t} = \mathbf{A}_0 \mathbf{P}_t + \mathbf{A}_1 \mathbf{P}_{t+\Delta t} + \mathbf{A}_d \mathbf{x}_t + \mathbf{A}_v \dot{\mathbf{x}}_t + \mathbf{A}_a \ddot{\mathbf{x}}_t, \quad (24)$$

with

$$\begin{aligned} \mathbf{A}_0 &= \frac{\Delta t^2}{6} \mathbf{C}_0, \\ \mathbf{A}_1 &= \frac{\Delta t^2}{6} \mathbf{C}_1, \\ \mathbf{A}_d &= \frac{\Delta t^2}{6} \mathbf{C}_d + \mathbf{I}, \\ \mathbf{A}_v &= \left(\frac{\Delta t}{6} \mathbf{C}_v + \mathbf{I} \right) \Delta t, \\ \mathbf{A}_a &= \frac{\Delta t^2}{6} (\mathbf{C}_a + 2\mathbf{I}). \end{aligned} \quad (25)$$

If \mathbf{x}_i , $\dot{\mathbf{x}}_i$, $\ddot{\mathbf{x}}_i$, and \mathbf{P}_i represent the displacement, velocity, acceleration, and excitation in equations (20)~(24) at time t_i , the relationship of the system responses between the two adjoining time steps t_{i+1} and t_i in the matrix form can be expressed as follows:

$$\begin{Bmatrix} \mathbf{x}_{i+1} \\ \dot{\mathbf{x}}_{i+1} \\ \ddot{\mathbf{x}}_{i+1} \end{Bmatrix} = \begin{bmatrix} \mathbf{A}_0 & \mathbf{A}_1 \\ \mathbf{B}_0 & \mathbf{B}_1 \\ \mathbf{C}_0 & \mathbf{C}_1 \end{bmatrix} \begin{Bmatrix} \mathbf{P}_i \\ \mathbf{P}_{i+1} \end{Bmatrix} + \begin{bmatrix} \mathbf{A}_d & \mathbf{A}_v & \mathbf{A}_a \\ \mathbf{B}_d & \mathbf{B}_v & \mathbf{B}_a \\ \mathbf{C}_d & \mathbf{C}_v & \mathbf{C}_a \end{bmatrix} \begin{Bmatrix} \mathbf{x}_i \\ \dot{\mathbf{x}}_i \\ \ddot{\mathbf{x}}_i \end{Bmatrix}, \quad (26)$$

and the response at time t_i can be also expressed as follows:

$$\begin{Bmatrix} \mathbf{x}_i \\ \dot{\mathbf{x}}_i \\ \ddot{\mathbf{x}}_i \end{Bmatrix} = \sum_{j=0}^{i-1} \begin{bmatrix} \mathbf{A}_d & \mathbf{A}_v & \mathbf{A}_a \\ \mathbf{B}_d & \mathbf{B}_v & \mathbf{B}_a \\ \mathbf{C}_d & \mathbf{C}_v & \mathbf{C}_a \end{bmatrix}^j \begin{bmatrix} \mathbf{A}_0 & \mathbf{A}_1 \\ \mathbf{B}_0 & \mathbf{B}_1 \\ \mathbf{C}_0 & \mathbf{C}_1 \end{bmatrix} \begin{Bmatrix} \mathbf{P}_{i-j-1} \\ \mathbf{P}_{i-j} \end{Bmatrix} + \begin{bmatrix} \mathbf{A}_d & \mathbf{A}_v & \mathbf{A}_a \\ \mathbf{B}_d & \mathbf{B}_v & \mathbf{B}_a \\ \mathbf{C}_d & \mathbf{C}_v & \mathbf{C}_a \end{bmatrix}^i \begin{Bmatrix} \mathbf{x}_0 \\ \dot{\mathbf{x}}_0 \\ \ddot{\mathbf{x}}_0 \end{Bmatrix}, \quad (27)$$

where i and j represent the power of the corresponding matrix, respectively. Equation (27) is a new explicit expression of the Wilson- θ method, and the responses of displacement, velocity, and acceleration in each time step can be solved simultaneously. Compared with the iterative algorithm, it is obvious that this explicit algorithm has more advantages. Letting $\mathbf{X}_i = \{\mathbf{x}_i^T, \dot{\mathbf{x}}_i^T, \ddot{\mathbf{x}}_i^T\}^T$ and assuming that the system is zero initial responses, that is, $\mathbf{X}_0 = 0$ and $\mathbf{P}_0 = 0$, then equation (27) can be rewritten as follows:

$$\mathbf{X}_i = \sum_{j=0}^{i-1} \begin{bmatrix} \mathbf{D}_j & \mathbf{E}_j \end{bmatrix} \begin{Bmatrix} \mathbf{P}_{i-j-1} \\ \mathbf{P}_{i-j} \end{Bmatrix}, \quad i = 1, 2, \dots, n, \quad (28)$$

with

$$\begin{aligned} \mathbf{D}_j &= \begin{bmatrix} \mathbf{A}_d & \mathbf{A}_v & \mathbf{A}_a \\ \mathbf{B}_d & \mathbf{B}_v & \mathbf{B}_a \\ \mathbf{C}_d & \mathbf{C}_v & \mathbf{C}_a \end{bmatrix}^j \begin{bmatrix} \mathbf{A}_0 \\ \mathbf{B}_0 \\ \mathbf{C}_0 \end{bmatrix}, \\ \mathbf{E}_j &= \begin{bmatrix} \mathbf{A}_d & \mathbf{A}_v & \mathbf{A}_a \\ \mathbf{B}_d & \mathbf{B}_v & \mathbf{B}_a \\ \mathbf{C}_d & \mathbf{C}_v & \mathbf{C}_a \end{bmatrix}^j \begin{bmatrix} \mathbf{A}_1 \\ \mathbf{B}_1 \\ \mathbf{C}_1 \end{bmatrix}. \end{aligned} \quad (29)$$

Assuming that \mathbf{y}_i denotes the measured responses of the system at time t_i , we obtain

$$\mathbf{y}_i = \mathbf{L}\mathbf{X}_i, \quad (30)$$

where \mathbf{L} is a $m_R \times 3n$ transformation matrix, in which m_R is the number of the measured response, and n is the number of degrees of freedom. The element of the k th column for the l th row of the \mathbf{L} matrix, which is corresponding to the l th measured response, is 1, and the other elements are 0. The value of k is

$$k = 3 \times (d-1) + r, \quad (31)$$

where d is corresponding to the d th degree of the measured response in the system and r is 1, 2, or 3, which represents that the measured response is displacement, velocity, and acceleration, respectively.

If there are m_F actual exciting forces in equation (1), that is, $\mathbf{F} = \{f_1, f_2, \dots, f_{m_F}\}^T$, which act on the l_1 th, l_2 th, \dots , l_{m_F} th masses, respectively, we obtain

$$\mathbf{P}_i = \mathbf{R}\mathbf{F}_i, \quad (32)$$

where \mathbf{R} is a $n \times m_F$ transformation matrix, in which the element of the k th column for the l_k th row of the \mathbf{R} matrix is 1, and the other ones are 0, $k = 1, 2, \dots, m_F$.

Inserting equation (32) into (28) and left multiplying it by \mathbf{L} , considering equation (30) and rearranging it, we obtain

$$\mathbf{y}_i = \begin{cases} \mathbf{W}_0 \mathbf{F}_1, & i = 1, \\ \sum_{j=1}^{i-1} (\mathbf{Q}_{i-j-1} + \mathbf{W}_{i-j}) \mathbf{F}_j + \mathbf{W}_0 \mathbf{F}_i, & i > 1, \end{cases} \quad (33)$$

with

$$\begin{aligned} \mathbf{Q}_j &= \mathbf{L}\mathbf{D}_j\mathbf{R}, \\ \mathbf{W}_j &= \mathbf{L}\mathbf{E}_j\mathbf{R}. \end{aligned} \quad (34)$$

Equation (33) can be written as a convolution form of matrices from time 1 to n :

$$\mathbf{Y} = \mathbf{H}\mathbf{F}, \quad (35)$$

with

$$\begin{aligned} \mathbf{Y} &= \begin{Bmatrix} \mathbf{y}_1 \\ \mathbf{y}_2 \\ \vdots \\ \mathbf{y}_n \end{Bmatrix}, \\ \mathbf{H} &= \begin{bmatrix} \mathbf{W}_0 & 0 & 0 & \dots & 0 \\ \mathbf{Q}_0 + \mathbf{W}_1 & \mathbf{W}_0 & 0 & \dots & 0 \\ \mathbf{Q}_1 + \mathbf{W}_2 & \mathbf{Q}_0 + \mathbf{W}_1 & \mathbf{W}_0 & \dots & 0 \\ \vdots & \vdots & \vdots & \ddots & \vdots \\ \mathbf{Q}_{n-2} + \mathbf{W}_{n-1} & \mathbf{Q}_{n-3} + \mathbf{W}_{n-2} & \mathbf{Q}_{n-4} + \mathbf{W}_{n-3} & \dots & \mathbf{W}_0 \end{bmatrix}, \\ \mathbf{F} &= \begin{Bmatrix} \mathbf{F}_1 \\ \mathbf{F}_2 \\ \vdots \\ \mathbf{F}_n \end{Bmatrix}. \end{aligned} \quad (36)$$

For a deterministic system, \mathbf{H} is a constant, and \mathbf{Y} can be obtained by measuring the response of the system. In fact, the measurement data \mathbf{Y} will be affected by the errors, such as measurement noise, truncation error, and principle error. Hence, the form of load identification with errors can be written as

$$\mathbf{Y} + \mathbf{w} = \mathbf{H}\mathbf{F}, \quad (37)$$

where \mathbf{w} denotes the error vector. The measurement data \mathbf{Y} are disturbed by errors. At this time, if the condition number of the core matrix \mathbf{H} is very large, the system will be seriously ill-posed. This means that the excitation \mathbf{F} is very sensitive to even a small error disturbance of the measured data \mathbf{Y} , so it is difficult to get an accurate excitation \mathbf{F} . In order to overcome the influence of ill-posed problems, the regularization method can be used to determine \mathbf{F} .

3. An Improved Regularization Algorithm

The regularization method is an effective means to solve ill-posed problems. The quality of the regularization method directly affects the accuracy of dynamic load identification results. Based on the Tikhonov regularization, an improved regularization method is proposed, and U-curve method is introduced to select the regularization parameter.

3.1. Tikhonov Regularization. In the load identification problem, the measurement data with noise, $\mathbf{Y}^\delta = \mathbf{Y} + \mathbf{w}$, should satisfy

$$\|\mathbf{Y}^\delta - \mathbf{Y}\| \leq \delta. \quad (38)$$

The purpose of Tikhonov regularization is to find the weighted minimum of the residual norm and solution norm in equation (39), so as to obtain the stable solution $\mathbf{F}^{\lambda, \delta}$ of the ill-posed inverse problem [14]:

$$\mathbf{F}^{\lambda, \delta} = \arg \min_{\mathbf{F}} \|\mathbf{H}\mathbf{F} - \mathbf{Y}^\delta\|^2 + \lambda \|\mathbf{F}\|^2, \quad (39)$$

where $\|\mathbf{H}\mathbf{F} - \mathbf{Y}^\delta\|^2$ denotes the l_2 -norm of residuals, λ denotes the regularization parameter, and $\lambda \|\mathbf{F}\|^2$ plays a role in regularizing ill-posed inverse. The norm term in equation (39) can be transformed into the matrix form:

$$\mathbf{J}(\mathbf{F}, \lambda) = \|\mathbf{H}\mathbf{F} - \mathbf{Y}^\delta\|^2 + \lambda \|\mathbf{F}\|^2 = [\mathbf{H}\mathbf{F} - \mathbf{Y}^\delta]^T [\mathbf{H}\mathbf{F} - \mathbf{Y}^\delta] + \lambda [\mathbf{F}]^T [\mathbf{F}]. \quad (40)$$

The regular solution of load identification $\mathbf{F}^{\lambda, \delta}$ can be obtained by finding the minimum of $\mathbf{J}(\mathbf{F}, \lambda)$:

$$\frac{\partial \mathbf{J}(\mathbf{F}, \lambda)}{\partial \mathbf{F}} = 2\mathbf{H}^T [\mathbf{H}\mathbf{F} - \mathbf{Y}^\delta] + 2\lambda \mathbf{F} = 0. \quad (41)$$

The regular solution $\mathbf{F}^{\lambda, \delta}$ should satisfy

$$(\mathbf{H}^T \mathbf{H} + \lambda \mathbf{I}) \mathbf{F}^{\lambda, \delta} = \mathbf{H}^T \mathbf{Y}^\delta. \quad (42)$$

The explicit unique solution of $\mathbf{F}^{\lambda, \delta}$ can be obtained from equation (42):

$$\mathbf{F}^{\lambda, \delta} = [\mathbf{H}^T \mathbf{H} + \lambda \mathbf{I}]^{-1} \mathbf{H}^T \mathbf{Y}^\delta. \quad (43)$$

3.2. Improved Regularization Algorithm. Inserting equation (32) into (26), left multiplying it by \mathbf{L} , considering equation (30), we obtain

$$\mathbf{y}_{i+1} = [\mathbf{Q}_0 \quad \mathbf{W}_0] \begin{Bmatrix} \mathbf{F}_i \\ \mathbf{F}_{i+1} \end{Bmatrix} + \mathbf{y}_{ri}, \quad (44)$$

where \mathbf{y}_{ri} denotes the responses of the initial condition for the system and is expressed as follows:

$$\mathbf{y}_{ri} = \mathbf{L} \begin{bmatrix} \mathbf{A}_d \mathbf{A}_v \mathbf{A}_a \\ \mathbf{B}_d \mathbf{B}_v \mathbf{B}_a \\ \mathbf{C}_d \mathbf{C}_v \mathbf{C}_a \end{bmatrix} \mathbf{X}_i. \quad (45)$$

Inserting $\mathbf{F}_{i+1} = \mathbf{F}_i + \Delta \mathbf{F}_i$ into equation (44) and rearranging it, we obtain

$$\mathbf{W}_0 \Delta \mathbf{F}_i = \mathbf{y}_{i+1} - \mathbf{y}_{ri} - \mathbf{y}_{Fi}, \quad (46)$$

with

$$\mathbf{y}_{Fi} = (\mathbf{W}_0 + \mathbf{Q}_0) \mathbf{F}_i. \quad (47)$$

Assuming that the measured response with noise is $\mathbf{y}_{i+1}^\delta = \mathbf{y}_{i+1} + \mathbf{w}_{i+1}$, and that $\mathbf{y}_{s(i+1)} = \mathbf{y}_{i+1} - \mathbf{y}_{Fi} - \mathbf{y}_{ri}$, the disturbance equation of (46) can be rewritten as follows:

$$\mathbf{W}_0 (\Delta \mathbf{F}_i + \Delta \mathbf{F}_{ni}) = \mathbf{y}_{s(i+1)} + \mathbf{w}_{i+1}, \quad (48)$$

where $\Delta \mathbf{F}_{ni}$ is the disturbance for the solution of equation (46).

According to Reference [32], we obtain

$$\frac{\|\Delta \mathbf{F}_{ni}\|}{\|\Delta \mathbf{F}_i\|} \leq \text{cond}(\mathbf{W}_0) \frac{\|\mathbf{w}_{i+1}\|}{\|\mathbf{y}_{s(i+1)}\|}, \quad (49)$$

where $\text{cond}(\mathbf{W}_0)$ is the condition number of the matrix \mathbf{W}_0 and expressed as follows:

$$\begin{aligned} \text{cond}(\mathbf{W}_0) &= \|\mathbf{W}_0\| \cdot \|\mathbf{W}_0^{-1}\| \\ &= \left(\max \frac{\|\mathbf{W}_0 \mathbf{z}\|}{\|\mathbf{z}\|} \right) \cdot \left(\min \frac{\|\mathbf{W}_0 \mathbf{z}\|}{\|\mathbf{z}\|} \right)^{-1}. \end{aligned} \quad (50)$$

If $\text{cond}(\mathbf{W}_0)$ is far greater than 1, effect of \mathbf{w}_{i+1} on the calculated result is enhanced. On the other hand, the state variables \mathbf{X}_i and force \mathbf{F}_i need to be calculated from the measured responses $\mathbf{y}_1^\delta, \mathbf{y}_2^\delta, \dots, \mathbf{y}_i^\delta$ during the process of load identification. Hence, $\Delta \mathbf{F}_i$ in equation (48) also consists of real increment, $\Delta \mathbf{F}_{Ri}$, of the exciting forces and pseudoincrement, $\Delta \mathbf{F}_{Pi}$, stemming from measurement noise and truncation error. The real increment of the exciting forces, $\Delta \mathbf{F}_{Ri}$, in interval of one sampling period is very small; that is, $\|\Delta \mathbf{F}_{Ri}\|$ approaches to 0 with increase of the sampling frequency. According to equations (48) and (49), one can deduce that $\Delta \mathbf{F}_{Pi} + \Delta \mathbf{F}_{ni}$ must be far greater than $\Delta \mathbf{F}_{Ri}$. Therefore, the least squares method of the ill-posed inverse problem Equation (37) can be expressed as follows:

$$\begin{aligned} &\text{minimize} \quad \|\mathbf{H}\mathbf{F} - \mathbf{Y}^\delta\|^2, \\ &\text{subject to} \quad \frac{1}{n} \|\Delta \mathbf{F}\|^2 \approx 0, \end{aligned} \quad (51)$$

where n denotes the sampling number. Classical penalty function methods [33] replace the constrained problem by an unconstrained problem of the form as follows:

$$\text{minimize} \quad \|\mathbf{H}\mathbf{F} - \mathbf{Y}^\delta\|^2 + \lambda' \frac{1}{n} \|\Delta \mathbf{F}\|^2. \quad (52)$$

Assuming that $\lambda = \lambda'/n$, we obtain

$$\mathbf{F}^{\lambda, \delta} = \arg \min_{\mathbf{F}} \|\mathbf{H}\mathbf{F} - \mathbf{Y}^\delta\|^2 + \lambda \|\Delta \mathbf{F}\|^2. \quad (53)$$

It is noticed that the solution $\Delta \mathbf{F}_i + \Delta \mathbf{F}_{ni}$ of equation (48) can also be obtained after solving equation (37) for \mathbf{F} . Under the zero initial conditions, that is, $\mathbf{X}_0 = 0$ and $\mathbf{F}_0 = 0$, $\Delta \mathbf{F}_i + \Delta \mathbf{F}_{ni}$ can be expressed as follows:

$$\Delta \mathbf{F} = \{ \mathbf{F}_1 - \mathbf{F}_0 \quad \mathbf{F}_2 - \mathbf{F}_1 \quad \cdots \quad \mathbf{F}_n - \mathbf{F}_{n-1} \}^T = \mathbf{N}\mathbf{F}, \quad (54)$$

with

$$\mathbf{N} = \begin{bmatrix} 1 & & & & & \\ -1 & 1 & & & & \\ & & \ddots & \ddots & & \\ & & & -1 & 1 & \\ & & & & -1 & 1 \end{bmatrix}. \quad (55)$$

Then, equation (53) can be transformed into

$$\mathbf{F}^{\lambda, \delta} = \arg \min_{\mathbf{F}} \left\| \mathbf{H}\mathbf{F} - \mathbf{Y}^\delta \right\|^2 + \lambda \|\mathbf{N}\mathbf{F}\|^2. \quad (56)$$

Comparing equation (56) with equations (39) and (56) is considered to be an improved regularization algorithm (IRA). Similar to the Tikhonov regularization method, the norm term in equation (56) can be transformed into the matrix form:

$$\begin{aligned} \mathbf{J}(\mathbf{F}, \lambda) &= \left\| \mathbf{H}\mathbf{F} - \mathbf{Y}^\delta \right\|^2 + \lambda \|\mathbf{F}\|^2 \\ &= [\mathbf{H}\mathbf{F} - \mathbf{Y}^\delta]^T [\mathbf{H}\mathbf{F} - \mathbf{Y}^\delta] + \lambda [\mathbf{N}\mathbf{F}]^T [\mathbf{N}\mathbf{F}]. \end{aligned} \quad (57)$$

The regular solution of load identification $\mathbf{F}^{\lambda, \delta}$ can be obtained by finding the minimum of $\mathbf{J}(\mathbf{F}, \lambda)$:

$$\frac{\partial \mathbf{J}(\mathbf{F}, \lambda)}{\partial \mathbf{F}} = 2\mathbf{H}^T [\mathbf{H}\mathbf{F} - \mathbf{Y}^\delta] + 2\lambda \mathbf{N}^T \mathbf{N}\mathbf{F} = 0. \quad (58)$$

The regular solution $\mathbf{F}^{\lambda, \delta}$ should satisfy

$$(\mathbf{H}^T \mathbf{H} + \lambda \mathbf{N}^T \mathbf{N}) \mathbf{F}^{\lambda, \delta} = \mathbf{H}^T \mathbf{Y}^\delta. \quad (59)$$

The explicit unique solution of $\mathbf{F}^{\lambda, \delta}$ can be obtained from the following equation:

$$\mathbf{F}^{\lambda, \delta} = [\mathbf{H}^T \mathbf{H} + \lambda \mathbf{N}^T \mathbf{N}]^{-1} \mathbf{H}^T \mathbf{Y}^\delta. \quad (60)$$

3.3. Determination of Regularization Parameters by U-Curve Method. The regularization method is actually a constrained least squares method. When the regularization parameter $\lambda = 0$, equations (40) and (60) are transformed into the least squares method. The selection of regularization parameters is very important. In fact, $\|\Delta \mathbf{F}\|_\infty$ is always greater than 0. Hence, if the value of λ is too large, the recognition error will increase; if the value of λ is too small, it will not play the role of regularization.

The principle of the U-curve method is similar to the L-curve method. The L-curve method [24] obtains the values of $\|\mathbf{H}\mathbf{F} - \mathbf{Y}^\delta\|$ and $\|\mathbf{N}\mathbf{F}\|$ at different values of λ . Then, a curve with $\log\|\mathbf{H}\mathbf{F} - \mathbf{Y}^\delta\|$ as the horizontal axis and $\log\|\mathbf{N}\mathbf{F}\|$ as the vertical axis is drawn. The shape of the curve is similar to the letter “L.” The optimum regularization parameter is the value of the position where the curvature of the curve is the largest (that is, the inflection point of the letter L). The U-curve method can be defined as follows [34]:

$$U(\lambda) = \frac{1}{\|\mathbf{H}\mathbf{F} - \mathbf{Y}^\delta\|^2} + \frac{1}{\|\mathbf{N}\mathbf{F}\|^2}, \quad (61)$$

with

$$\begin{aligned} \|\mathbf{H}\mathbf{F} - \mathbf{Y}^\delta\|^2 &= \sum_{i=1}^r \frac{\lambda^4 \psi_i^2}{(\sigma_i^2 + \lambda^2)^2}, \\ \|\mathbf{N}\mathbf{F}\|^2 &= \sum_{i=1}^r \frac{\sigma_i^2 \psi_i^2}{(\sigma_i^2 + \lambda^2)^2}, \end{aligned} \quad (62)$$

where $\boldsymbol{\psi} = \mathbf{u}^T \mathbf{Y}^\delta$, \mathbf{u} is the left singular value matrix after the singular value decomposition of the kernel function matrix \mathbf{H} . $\sigma_1 \geq \sigma_2 \geq \cdots \geq \sigma_r > 0$ is the singular value of matrix \mathbf{H} . The singular values of matrix \mathbf{N} are all 1. Because the image of $U(\lambda)$ is similar to the letter “U,” it is known as the U-curve method. The purpose of the U-curve criterion is to select the parameters whose curvature reaches the local maximum of the left vertical part of the U-curve, where the value λ is the best regularization parameter. Because the U-curve method has less computation, it is superior to the L-curve method in calculating speed.

4. Numerical Example

In this section, a multi-degree-of-freedom vibrating system is used to verify the effectiveness of the proposed method in comparison with the Tikhonov regularization method. Through the numeric simulations, the impact and harmonic loads of the system are identified using the IRA and the Tikhonov regularization, respectively. The effects of the sampling frequency and noise level on the errors of load identification are discussed.

The error between the recognition result and the real load is calculated through the following equation:

$$\begin{aligned} \mathbf{error} 1 &= \frac{|\mathbf{F}_{id} - \mathbf{F}_{real}|}{\|\mathbf{F}_{real}\|} \times 100\%, \\ \mathbf{error} 2 &= \frac{\|\mathbf{F}_{id} - \mathbf{F}_{real}\|}{\|\mathbf{F}_{real}\|} \times 100\%, \end{aligned} \quad (63)$$

where **error 1** denotes the relative error, **error 2** denotes the relative accumulation error, \mathbf{F}_{id} denotes the recognized load, \mathbf{F}_{real} denotes the real force, $|\cdot|$ denotes the absolute value, and $\|\cdot\|$ denotes the l_2 -norm.

Figure 2 shows a four-degree-of-freedom system, in which masses are $m_1 = 4258$ kg, $m_2 = 2258$ kg, $m_3 = 2437$ kg, and $m_4 = 1729$ kg, respectively. The stiffness is $k = 8.64 \times 10^6$ N/m. The damping is the Rayleigh damping, and the constants are $\alpha_1 = 0.1$ and $\alpha_2 = 3.6157 \times 10^{-4}$.

An impact load and the harmonic load are applied to the third degree of freedom of the system, respectively. The impact load is

$$f(t) = 30e^{(-2\pi p_0(t-0.8)^2)}, \quad (64)$$

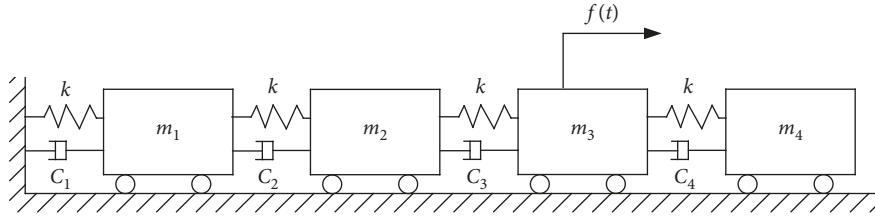


FIGURE 2: Four-degree-of-freedom system.

where parameter p_0 can adjust the frequency band of the impact load, and the peak value of the impact load appears at 0.8 s.

Harmonic load is

$$f(t) = 500 \sin(10\pi t). \quad (65)$$

In engineering, the measured responses of the system are inevitably disturbed by environmental noise. In order to simulate the measured data with noise, pseudorandom noise with uniform distribution is added to the displacement response. Hence, the displacement response is expressed as follows [35]:

$$\tilde{\mathbf{Y}} = \mathbf{Y} + \mathbf{e} = \mathbf{Y} + l_{\text{noise}} \cdot \text{std}(\mathbf{y}) \cdot (2\text{rand}(n, 1) - 1), \quad (66)$$

where l_{noise} denotes the noise level, which is chosen as 10%, 20%, and 30%, respectively. $\text{std}(\cdot)$ is a MATLAB script function that represents the standard deviation of vectors. The script function of MATLAB, $\text{rand}(n, 1)$, can get a random vector of $n \times 1$, which represents the pseudorandom values in the standard uniform distribution on the interval of $[0, 1]$.

Using the Newmark- β algorithm, equation (1) can be numerically calculated to obtain displacement responses of the system. Time step is 0.001 s, and the calculating time is 3 s. Figures 3 and 4 show the displacement responses of m_2 before and after adding 20% noise under the impact load and the harmonic load, respectively.

Herein, the displacement responses with noise in Figures 3 and 4 are used to identify the impact load and harmonic loads, respectively. The condition number of kernel function matrix \mathbf{H} is $3.44e+23$. In this case, matrix \mathbf{W}_0 is a scalar with a value of $1.095e-12$. According to equation (48), the error items, including the current measurement noise \mathbf{w}_{i+1} and calculated errors in $\mathbf{y}_{s(i+1)}$, will be amplified by $9.13e11$ times. These facts mean that the load identification problem of the system is seriously ill-posed. Using the U-curve method, the regularization parameter of the impact responses, λ , is determined to be $2e-12$ and $3e-15$ for the IRA and the Tikhonov regularization method, respectively; that of the harmonic response is $5e-13$ and $6e-15$ for the IRA and the Tikhonov regularization method, respectively. The condition numbers of the kernel function matrix regularized by the IRA and the Tikhonov regularization method are $1.88e+3$ and $9.45e+3$, respectively. Figure 5 shows comparisons of the identified loads with the real ones, and the relative errors between the recognition result and the real load for the IRA and the Tikhonov

regularization method are shown in Figure 6. As illustrated in Figures 5 and 6, the error of the identified load for the IRA is smaller than that for the Tikhonov regularization, except for the end segment of load identification.

In order to draw a performance comparison between the IRA and the Tikhonov regularization, Tables 1 and 2 list the regularization parameter and relative accumulation errors of identified loads for impact and harmonic loads under different sampling frequencies and different noise levels, respectively.

As shown in Tables 1 and 2, the regularization parameter of the IRA is much bigger than that of the Tikhonov regularization method. Furthermore, the regularization parameters of the two algorithms all increase with increases of the sampling frequency and the noise level. But the difference of regularization parameters for the two algorithms also increases with increases of the sampling frequency and the noise level.

The reason is that the single step increment of real exciting forces decreases with increase of the sampling frequency in comparison with the values of real exciting forces. Because eigenvalues of matrix \mathbf{N} in equation (56) are the same as that of a unit matrix in equation (39), the condition number of kernel function matrix \mathbf{H} regularized by the IRA must be much smaller than that regularized by the Tikhonov regularization method. Hence, relative accumulation errors of loads identified by the IRA are smaller than that by the Tikhonov regularization method. These facts demonstrate that noise resistance of the IRA is higher than that of the Tikhonov regularization and that the IRA is suitable to deal with complicated structures with huge sizes of mass and stiffness matrices as the same as the Tikhonov regularization method.

5. Experimental Verification

5.1. Experimental Setup. The experiments applied for load identification were conducted on an experimental system of vibration dynamics (model YE63251), as illustrated in Figure 7. The system consists of an electric activator (model YE15400), an impact hammer (model LC-10A) including a force sensor (model CL-YD-303A) and an electric eddy current displacement sensor (model CWY-DO-502), and a cantilever beam. The parameters of the cantilever beam are listed in Table 3, and the first four natural frequencies of the cantilever beam are 15.9 Hz, 99.8 Hz, 279.5 Hz, and 547.7 Hz, respectively.

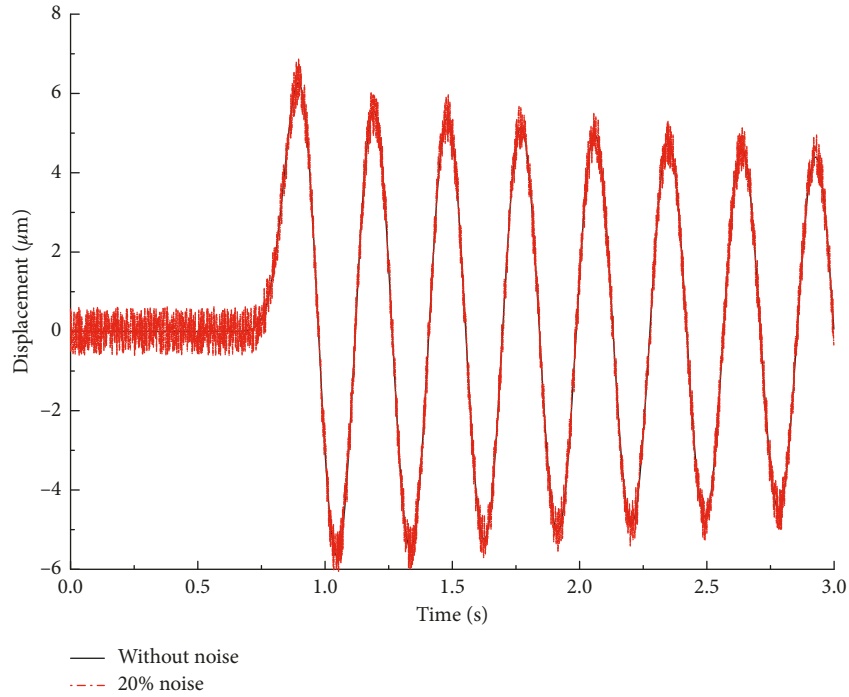


FIGURE 3: Displacement response of m_2 for the system excited by the impact load before and after adding 20% noise.

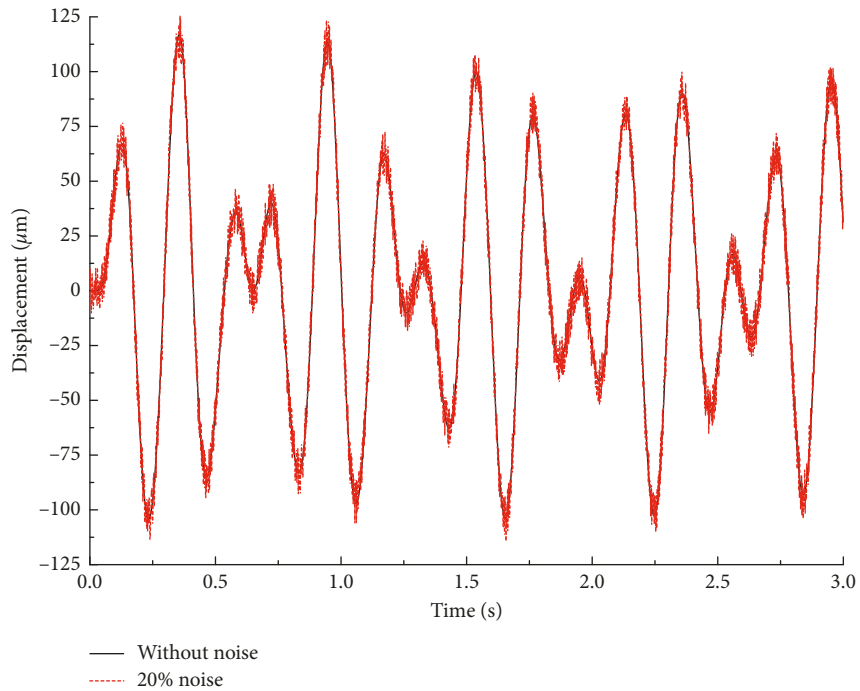


FIGURE 4: Displacement response of m_2 for the system excited by the harmonic load before and after adding 20% noise.

5.2. Theoretical Model. In order to identify load of the beam using the corresponding response, the dynamic model is set up by virtue of FEM. The cantilever beam is assumed to be a plane one and divided into 18 segments, as shown in Figure 8(b). As described by Hu and Wang [36], assuming that x -axis and y -axis represent the global coordinate system, the nodal displacements are grouped in the vector:

$$\mathbf{d}^e = [v_i \ \theta_i \ v_j \ \theta_j]^T, \quad (67)$$

where v represents the translational dof and θ denotes the rotational dof.

The element stiffness matrix (\mathbf{K}^e) and the element mass matrix (\mathbf{M}^e) are expressed as follows:

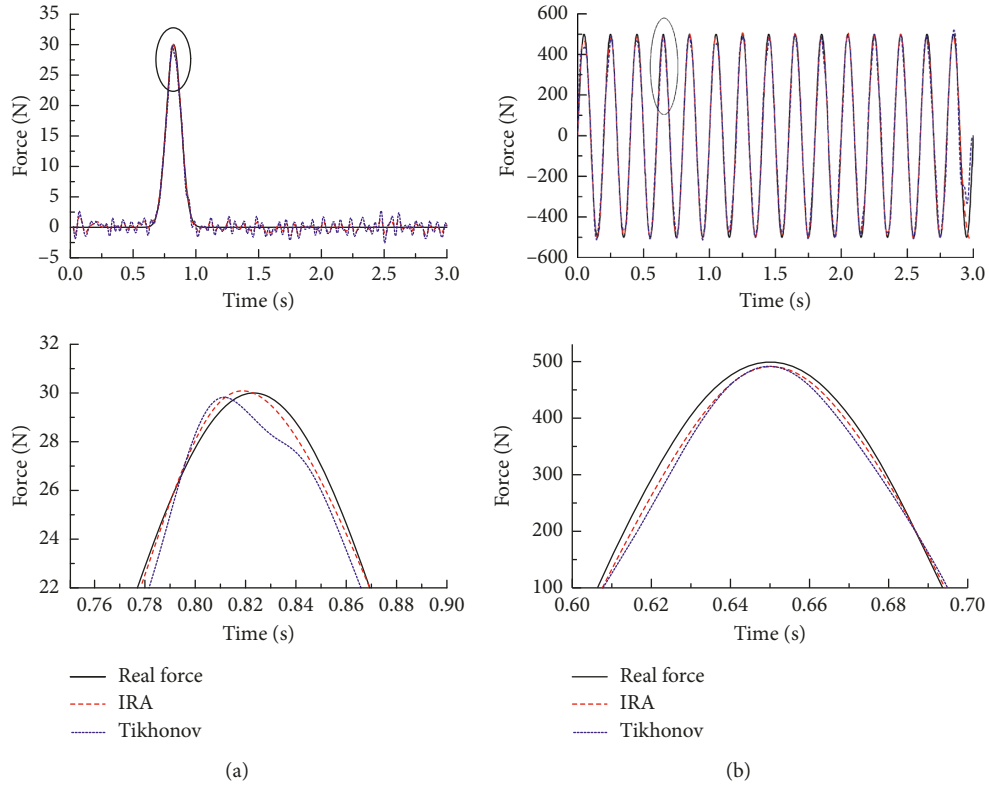


FIGURE 5: Loads identified by the responses with noise level of 20%: (a) impact load and (b) harmonic load.

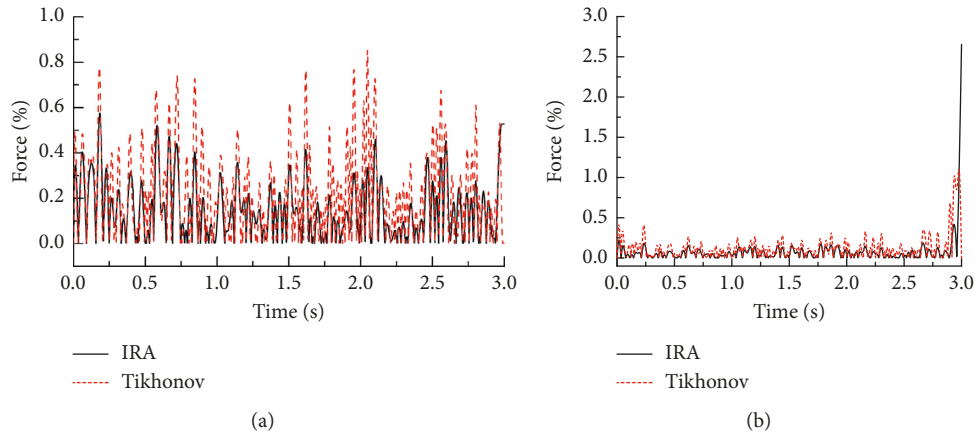


FIGURE 6: Relative errors identified by the responses with noise level of 20%: (a) impact load and (b) harmonic load.

TABLE 1: Regularization parameters and relative accumulation errors of the impact load.

Sampling frequency (Hz)	Noise level (%)	Regularization parameter		Error (%)	
		IRA	Tikhonov	IRA	Tikhonov
500	0	$1e-15$	$1e-16$	0.183671	0.230995
	10	$1e-13$	$1e-15$	4.144848	8.688246
	20	$8e-13$	$1e-15$	6.174314	12.484741
	30	$1e-12$	$2e-15$	8.438775	19.757432
1000	0	$1e-15$	$1e-16$	0.064986	0.160739
	10	$1e-12$	$1e-15$	2.557199	6.518704
	20	$2e-12$	$3e-15$	5.923524	10.009010
	30	$2.7e-12$	$5e-15$	9.163410	17.801819
2000	0	$1e-15$	$1e-16$	0.179296	2.679824
	10	$8e-13$	$1e-15$	2.836595	3.899927
	20	$1e-12$	$5e-15$	7.202332	8.112095
	30	$2e-12$	$7e-15$	11.814816	12.270310

TABLE 2: Regularization parameters and relative accumulation errors of harmonic load.

Sampling frequency (Hz)	Noise level (%)	Regularization parameter		Error (%)	
		IRA	Tikhonov	IRA	Tikhonov
500	0	$1e-16$	$1e-17$	0.951661	3.896035
	10	$1e-14$	$2e-15$	3.087554	5.168342
	20	$5e-13$	$2e-15$	5.093864	9.398055
	30	$1e-12$	$3e-15$	7.489087	11.361723
1000	0	$1e-16$	$1e-17$	0.166175	0.20726
	10	$1e-14$	$2e-15$	2.119125	4.458908
	20	$5e-13$	$6e-15$	3.797509	7.188128
	30	$1e-12$	$3e-15$	5.182875	10.441882
2000	0	$1e-14$	$1e-16$	0.099846	0.316657
	10	$1e-13$	$1e-15$	2.02805	3.813177
	20	$5e-13$	$6e-15$	2.582656	5.145480
	30	$4e-12$	$5e-15$	3.340285	8.215345

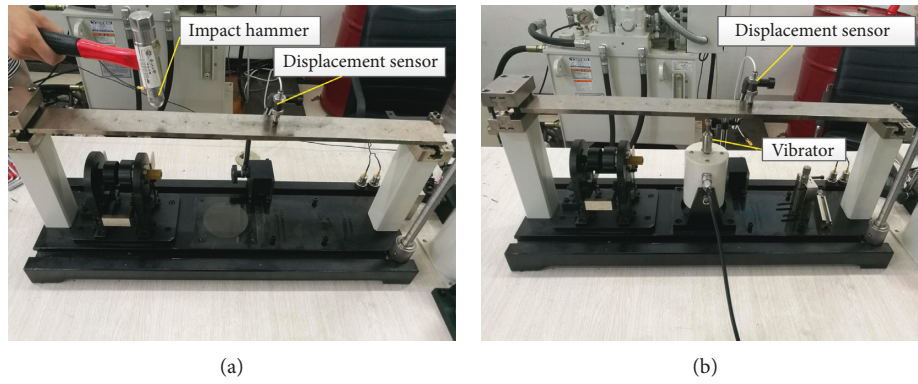


FIGURE 7: Experimental system of cantilever beam: (a) impact load and (b) harmonic load.

TABLE 3: Parameters of the cantilever beam.

Young's modulus, E	200 GPa
Density, ρ	7840 kg/m^3
Poisson's ratio, μ	0.33
Length, L	0.64 m
Width, b	0.056 m
Height, h	0.008 m

$$\mathbf{K}^e = \frac{EI_z}{l^3} \begin{bmatrix} 12 & 6l & -12 & 6l \\ 6l & 4l^2 & -6l & 2l^2 \\ -12 & -6l & 12 & -6l \\ 6l & 2l^2 & -6l & 4l^2 \end{bmatrix}, \quad (68)$$

$$\mathbf{M}^e = \frac{\rho A_J l}{420} \begin{bmatrix} 156 & 22l & 54 & -13l \\ 22l & 4l & 13l & -3l^2 \\ 54 & 13l & 156 & -22l \\ -13l & -3l^2 & -22l & 4l^2 \end{bmatrix},$$

where I_z denotes the moment of inertia, $I_z = bh^3/12$; A_J denotes the cross-sectional area, $A_J = bh$; and $l = L/18$ denotes the length of the beam element.

According to the finite element theory, the element stiffness matrix \mathbf{K}^e and the element mass matrix \mathbf{M}^e are integrated into the total stiffness matrix \mathbf{K} and the total mass matrix \mathbf{M} , respectively [36]. Then, the dynamic equations of the system can be expressed as follows:

$$\mathbf{M}\ddot{\mathbf{d}} + (\alpha_1\mathbf{M} + \alpha_2\mathbf{K})\dot{\mathbf{d}} + \mathbf{K}\mathbf{d} = 0. \quad (69)$$

Using matrices \mathbf{M} and \mathbf{K} , the natural frequencies of the beam were determined. The first five natural frequencies are listed in the second row of Table 4.

In order to determine the parameters of the finite element model, a hammer impact test was conducted to record impact load and displacement response, as shown in Figure 7(a). The hammer excited the beam at node 10, and the displacement sensor was located at node 12. Figure 9 shows the response of the beam for the hammer impact and its FFT results. The hammer impact excited only the first two natural frequencies, 15.6 Hz and 98.9 Hz, as shown in Figure 9(b). These values were slightly smaller than their theoretical ones, as shown in Table 4. The fact stems from the contact stiffness of clamped end of the cantilever beam. As shown in Figure 9(a), the amplitude envelope line of the response was approximately an exponential decay. This fact demonstrates that damping of the system is Rayleigh damping. According to the experimental results in [37], the hammer impact excites the free vibration frequencies of the system, which can be expressed as follows:

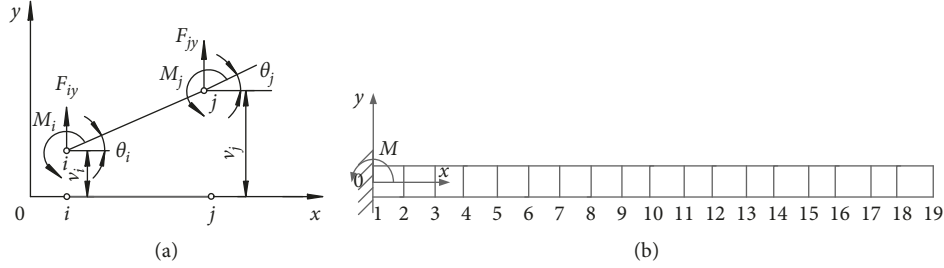


FIGURE 8: Structure diagram of cantilever beam: (a) planar beam element and (b) distribution of nodes for the cantilever beam.

TABLE 4: Comparison of natural frequencies for technical manual, theoretical, and measured values (Hz).

Mode	1st	2nd	3rd	4th
Technical manual	15.9	99.8	297.5	547.7
Theoretical values	15.7	99.4	296.9	547.1
Measured values	15.6	98.9	—	—

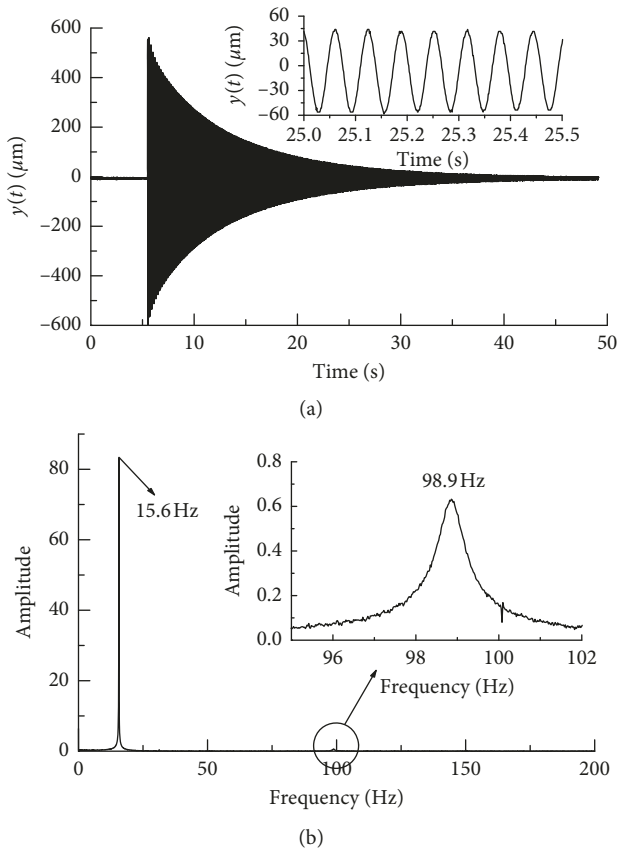


FIGURE 9: Impact response of the cantilever beam and its FFT results: (a) impact response and (b) FFT results.

$$y(t) = A_0 e^{-\xi \omega_n t} \sin(\omega_d t + \gamma), \quad (70)$$

with

$$\omega_d = \omega_n \sqrt{1 - \xi^2}. \quad (71)$$

In comparison with the amplitude of component 15.6 Hz, that of component 98.9 Hz is very small and can be

neglected. So, the relationship between the amplitude of $y(t)$ and time t can be expressed as follows:

$$\text{Amp}(y(t)) = A_0 e^{-\xi_1 \omega_{n1} t},$$

or

$$\ln(\text{Amp}(y(t))) = a_0 - b_0 t,$$

where $a_0 = \ln A_0$ and $b_0 = \xi_1 \omega_{n1}$.

The amplitude data were extracted from the displacement response in Figure 10(a) in the range of 6 s to 38 s. Then, the data of $\ln(\text{Amp}(y(t)))$ were linearly fitted using the least square method, and the results were shown in Figure 10. The coefficients of the linear fitting were $a_0 = 6.04$ and $b_0 = 0.1117$, that is, $\xi_1 \omega_{n1} = 0.1117$. Using equation (71), the natural frequency and the critical damping ratio of the first mode for the cantilever beam were determined to be 15.6 Hz and 0.00114, respectively. Taking the natural frequency of the second mode as 99.4 Hz, the critical damping ratio of the second mode is determined to be $\xi_2 = 0.1002$ using equation (71).

Using equation (3), we get linear equations as follows:

$$\frac{\alpha_1}{62.4\pi} + 15.6\pi\alpha_2 = 0.00114, \quad (73)$$

$$\frac{\alpha_1}{397.6\pi} + 99.4\pi\alpha_2 = 0.1002.$$

Solving equation (73) for α_1 and α_2 , we obtain

$$\alpha_1 = -2.9315, \quad (74)$$

$$\alpha_2 = 3.2839 \times 10^{-4}.$$

In order to ensure the fidelity between the finite element model and the actual specimen, a harmonic exciting test was also conducted to record exciting force and the displacement response, as shown in Figure 7(b). The electric activator excited the beam at node 10, and the displacement sensor was located at node 12. Using the Newmark- β algorithm, Equation (69) was simulated to determine the displacement responses excited by the impact load and the harmonic load, respectively. Figures 11(a) and 11(b) show comparisons of the simulation result with the experimental result for the impact and harmonic loads, which reveal quite well agreement, respectively.

5.3. Load Identifications. Through the data of displacement responses in Figure 11, the impact and harmonic loads of the

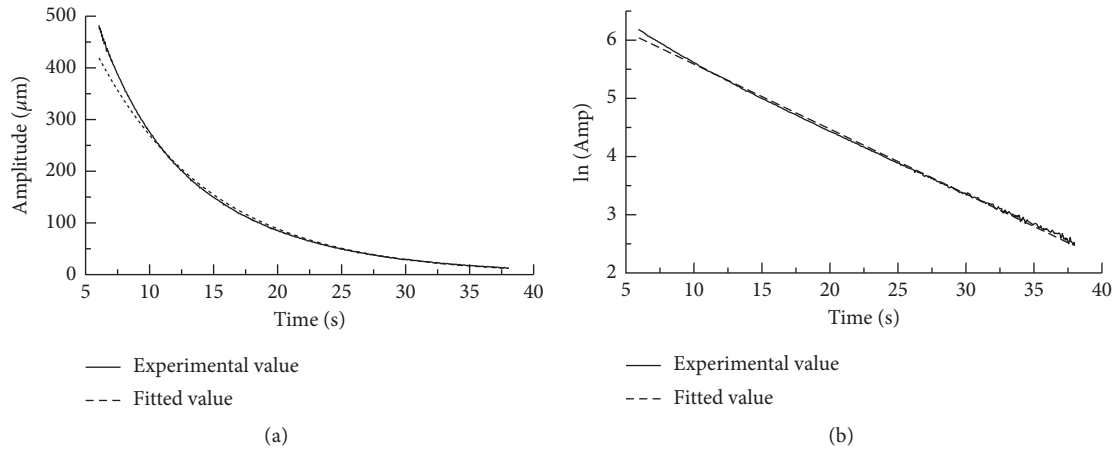


FIGURE 10: Curve fittings of amplitude for the impact response: (a) power function curve fitting and (b) linear fitting.

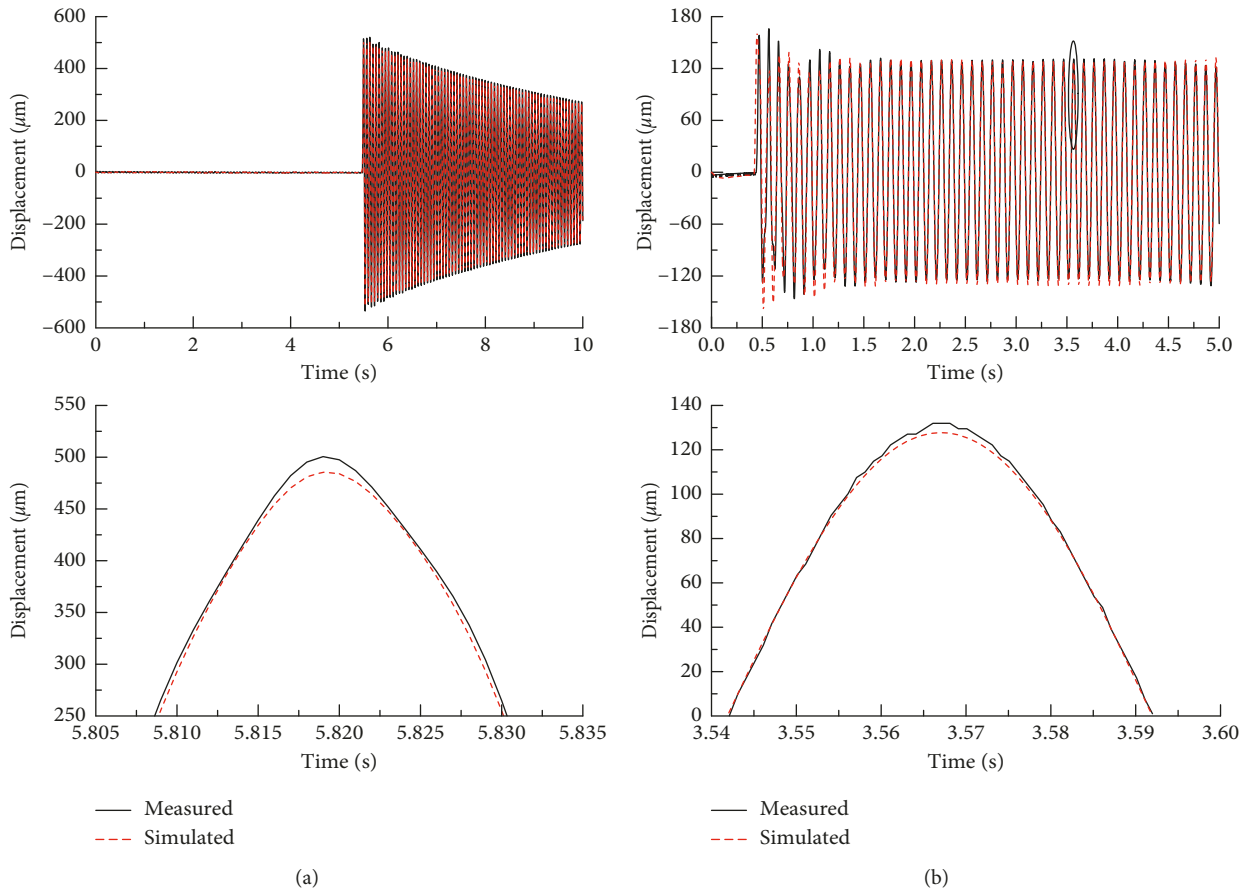


FIGURE 11: Comparisons of the simulation result with the experimental result: (a) impact load and (b) harmonic load.

system were identified using the IRA and the Tikhonov regularization method, respectively. The identified results of impact load are shown in Figure 12, and that of harmonic load and its FFT result are shown in Figure 13. Furthermore, the measured point of displacement response stayed at the point of node 12, tests of excited point at the points of nodes 4, 6, and 15 for impact and harmonic loads were conducted to record the exciting force and the corresponding

displacement response, respectively. Then, the excited loads were identified using the IRA and the Tikhonov regularization method, respectively.

Tables 5 and 6 show comparisons of the IRA with the Tikhonov regularization method for the regularization parameters and the relative accumulation errors of impact and harmonic loads, respectively. As the same as the simulation results in Tables 1 and 2, the regularization parameter of the

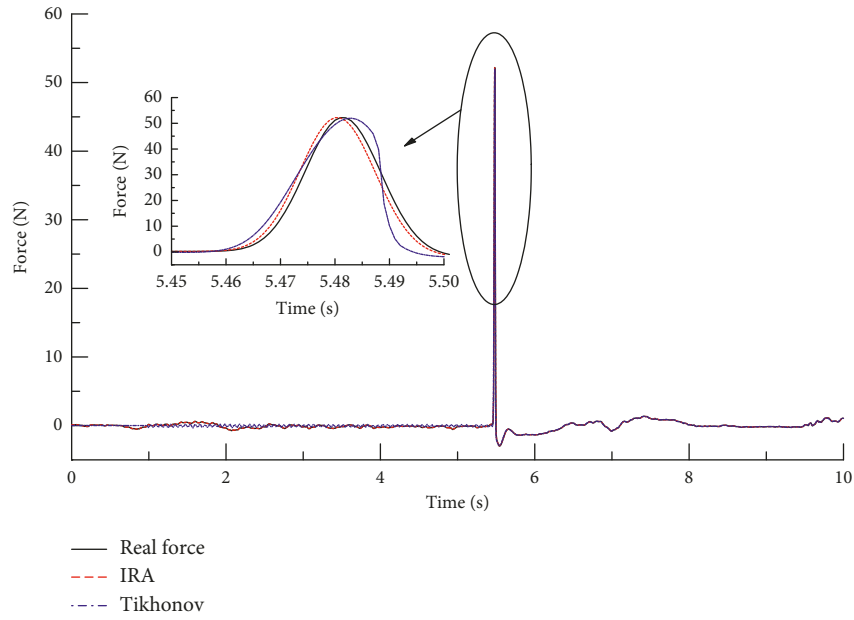


FIGURE 12: Identified results of the impact load.

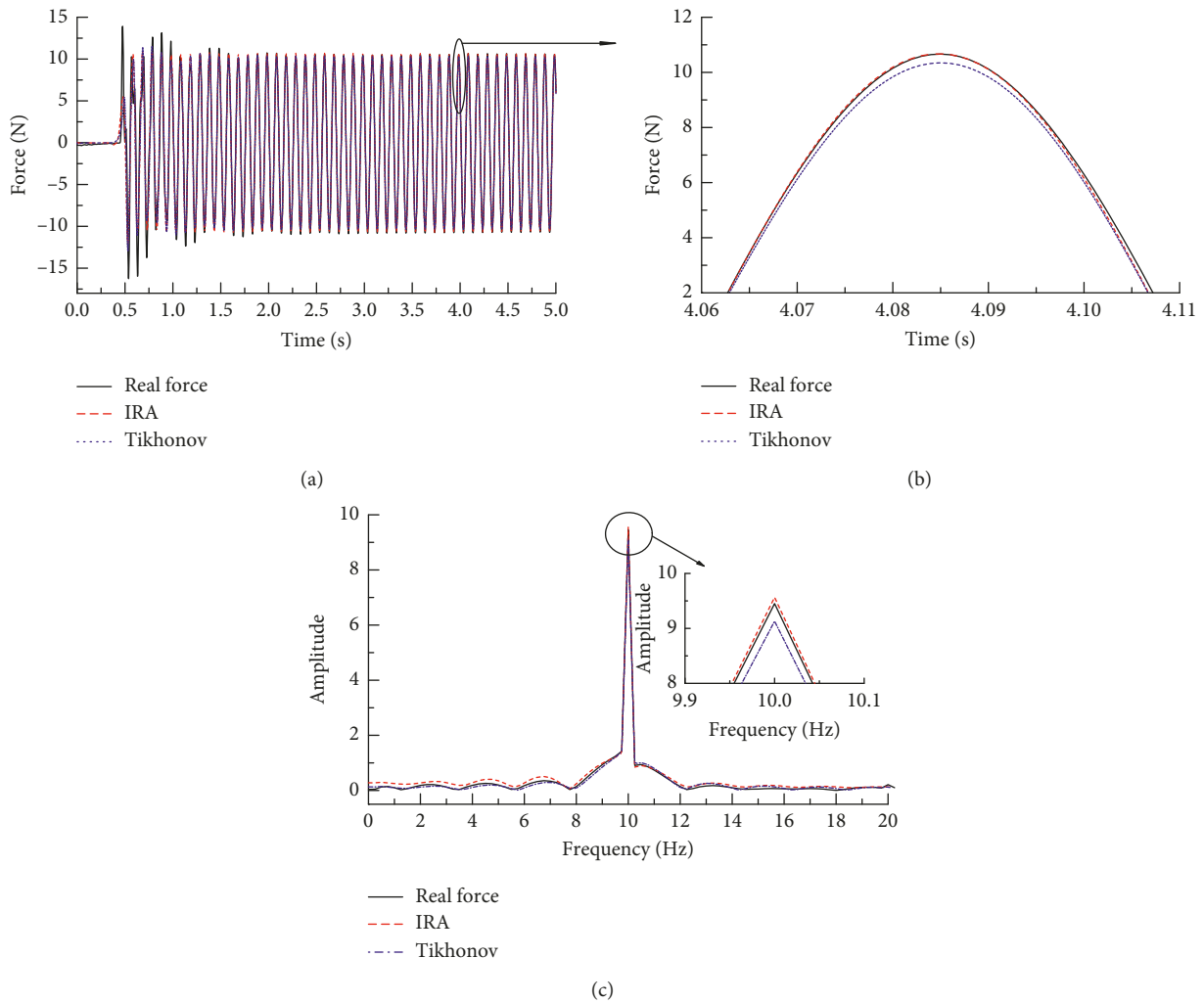


FIGURE 13: Identified result of the harmonic loads and its frequency spectrum.

TABLE 5: Comparisons of the IRA with the Tikhonov regularization for the identified impact load errors under differential exciting points.

Excitation points	Condition number	Regularization parameter		Error (%)	
		IRA	Tikhonov	IRA	Tikhonov
6	4.7258e6	6.2546e-9	3.6244e-11	4.651456	8.558625
8	4.9454e6	3.2258e-9	2.6716e-11	3.869557	7.776456
10	5.5213e6	4.5743e-9	1.5416e-11	3.568851	7.216584
15	5.8876e6	6.2538e-9	5.2264e-11	4.655242	8.588946

TABLE 6: Comparisons of the IRA with the Tikhonov regularization for the identified harmonic load errors under differential excited points.

Excitation points	Condition number	Regularization parameter		Error (%)	
		IRA	Tikhonov	IRA	Tikhonov
4	4.5079e6	7.4715e-11	2.8212e-13	3.298616	4.298616
10	5.1510e6	2.9021e-9	1.2324e-11	3.414175	4.625209
12	5.5405e6	3.5235e-9	1.4592e-11	3.239187	4.252354
15	6.1644e6	8.8048e-9	3.7205e-11	2.348616	5.474881

IRA is much bigger than that of the Tikhonov regularization method and the relative accumulation errors of loads identified by the virtue of the IRA are smaller than that by the virtue of the Tikhonov regularization. All the above facts demonstrate that the performance of the IRA proposed in this paper is better than that of the Tikhonov regularization method for load identification.

6. Conclusions

This paper gives a general explicit form of the Wilson- θ algorithm to identify dynamic loads. Then, an improved regularization algorithm is proposed to solve the ill-posed problem of dynamic load identification instead of the Tikhonov regularization method. The main novelty of the IRA is that it replaces l_2 -norm of the exciting force vector with that of the increment vector for the exciting force. Compared with the Tikhonov regularization method through the computer simulations and the experiments for identifications of impact and harmonic loads, the regularization parameter of the IRA is much bigger than that of the Tikhonov regularization method. Furthermore, the regularization parameters of the two algorithms all increase with increases of the sampling frequency and the noise level. But the difference of regularization parameters for the two algorithms also increases with increases of the sampling frequency and the noise level. Therefore, the performance of the IRA is better than that of the Tikhonov regularization method for load identification. Because all the eigenvalues of the transformation matrix between the exciting force vector and its increment vector are the same as that of an unit matrix, the IRA is suitable to deal with complicated structures with huge sizes of mass and stiffness matrices as the same as the Tikhonov regularization method.

Data Availability

The data used to support the findings of this study are available from the corresponding author upon request.

Conflicts of Interest

The authors declare that they have no conflicts of interest.

Acknowledgments

This work was supported by the National Natural Science Foundation of China (no. 51775094).

References

- [1] M. Ghajari, Z. Sharif-Khodaei, M. H. Aliabadi, and A. Apicella, "Identification of impact force for smart composite stiffened panels," *Smart Materials and Structures*, vol. 22, no. 8, article 085014, 2013.
- [2] J. Park, S. Ha, and F.-K. Chang, "Monitoring impact events using a system-identification method," *AIAA Journal*, vol. 47, no. 9, pp. 2011–2021, 2009.
- [3] H. Innoue, J. Harrigan, and S. Reid, "Review of inverse analysis for indirect measurement of impact force," *Applied Mechanics Reviews*, vol. 54, no. 6, pp. 503–524, 2001.
- [4] D. J. Ewins, *Modal Testing: Theory, Practice and Application*, Research Studies Press Ltd., Baldock, UK, 2nd edition, 2000.
- [5] L. Wang, X. Han, and Y. Xie, "A new conjugate gradient method for solving multi-source dynamic load identification problem," *International Journal of Mechanics and Materials in Design*, vol. 9, no. 3, pp. 191–197, 2013.
- [6] J. Liu, X. Sun, K. Li, and C. Jiang, "A probability density function discretization and approximation method for the dynamic load identification of stochastic structures," *Journal of Sound and Vibration*, vol. 357, pp. 74–94, 2015.
- [7] A. N. Han and D. J. Thompson, "The quantification of structure-borne transmission paths by inverse methods. Part 1: improved singular value rejection methods," *Journal of Sound and Vibration*, vol. 264, no. 2, pp. 411–431, 2003.
- [8] A. N. Thite and D. J. Thompson, "The quantification of structure-borne transmission paths by inverse methods. Part 2: use of regularization techniques," *Journal of Sound and Vibration*, vol. 264, no. 2, pp. 433–451, 2003.
- [9] H. G. Choi, A. N. Thite, and D. J. Thompson, "A threshold for the use of Tikhonov regularization in inverse force determination," *Applied Acoustics*, vol. 67, no. 7, pp. 700–719, 2006.

- [10] H. Inoue, K. Kishimoto, T. Shibuya, and T. Koizumi, "Estimation of impact force by an inverse analysis," in *Inverse Problem in Engineering Mechanics*, pp. 169–178, Elsevier, Amsterdam, Netherlands, 1993.
- [11] H. Inoue, K. Kishimoto, T. Shibuya, and K. Harada, "Regularization of numerical inversion of the Laplace transform for the inverse analysis of impact force," *JSME International Journal Series A*, vol. 41, no. 4, pp. 473–480, 1998.
- [12] E. Jacquelin, A. Bennani, and P. Hamelin, "Force reconstruction: analysis and regularization of a deconvolution problem," *Journal of Sound and Vibration*, vol. 265, no. 1, pp. 81–107, 2003.
- [13] R. Adams and J. F. Doyle, "Multiple force identification for complex structures," *Experimental Mechanics*, vol. 42, no. 1, pp. 25–37, 2000.
- [14] J. Liu, X. Meng, C. Jiang, and X. Han, "Time-domain Galerkin method for dynamic load identification," *International Journal for Numerical Methods in Engineering*, vol. 105, no. 8, pp. 620–640, 2016.
- [15] J. Zhang, X. Meng, D. Zhang, C. Jiang, and X. Han, "An efficient method to reduce ill-posedness for structural dynamic load identification," *Mechanical Systems and Signal Processing*, vol. 95, pp. 273–285, 2017.
- [16] B. Qiao, X. Zhang, C. Wang, H. Zhang, and X. Chen, "Sparse regularization for force identification using dictionaries," *Journal of Sound and Vibration*, vol. 368, pp. 71–86, 2016.
- [17] B. Qiao, X. Zhang, X. Luo, and X. Chen, "A force identification method using cubic B-spline scaling functions," *Journal of Sound and Vibration*, vol. 337, pp. 28–44, 2015.
- [18] B. Qiao, X. Chen, X. Xue, X. Luo, and R. Liu, "The application of cubic B-spline collocation method in impact force identification," *Mechanical Systems and Signal Processing*, vol. 64–65, pp. 413–427, 2015.
- [19] B. Qiao, X. Zhang, J. Gao, R. Liu, and X. Chen, "Sparse deconvolution for the large-scale ill-posed inverse problem of impact force reconstruction," *Mechanical Systems and Signal Processing*, vol. 83, pp. 93–115, 2016.
- [20] B. Qiao, Z. Mao, J. Liu, Z. Zhao, and X. Chen, "Group sparse regularization for impact force identification in time domain," *Journal of Sound and Vibration*, vol. 445, pp. 44–63, 2019.
- [21] L. Wang, Y. Xie, Z. Wu, Y. Du, and K. He, "A new fast convergent iteration regularization method," *Engineering with Computers*, vol. 35, no. 1, pp. 127–138, 2018.
- [22] J. Liu, X. Sun, X. Meng, K. Li, G. zeng, and X. Wang, "A novel shape function approach of dynamic load identification for the structures with interval uncertainty," *International Journal of Mechanics and Materials in Design*, vol. 12, no. 3, pp. 1–12, 2015.
- [23] J. Liu, X. Sun, X. Han, C. Jiang, and D. Yu, "Dynamic load identification for stochastic structures based on Gegenbauer polynomial approximation and regularization method," *Mechanical Systems and Signal Processing*, vol. 56–57, pp. 35–54, 2015.
- [24] O. ' Leary, D. Prost, and P. C. Hansen, "The use of the L-curve in the regularization of discrete ill-posed problems," *SIAM Journal on Scientific Computing*, vol. 14, no. 6, pp. 1487–1503, 1993.
- [25] Y. Lu and Z. Wang, "Determination of ridge parameters in ridge estimate by U-curve method," *Journal of Navigation*, vol. 3, pp. 132–134, 2015.
- [26] P. Xu and J. R. Geophys, "Truncated SVD methods for discrete linear ill-posed problems," *Geophysical Journal International*, vol. 135, no. 2, pp. 505–514, 2010.
- [27] L. Wang, X. Zhao, and H. Gao, "A method for determining the regularization parameter and the relative weight ratio of the seismic slip distribution with multi-source data," *Journal of Geodynamics*, vol. 118, no. 7, pp. 1–10, 2018.
- [28] Y. Jia, Z. Yang, N. Guo, and L. Wang, "Random dynamic load identification based on error analysis and weighted total least squares method," *Journal of Sound and Vibration*, vol. 358, pp. 111–123, 2015.
- [29] Y. Jia, Z. Yang, and Q. Song, "Experimental study of random dynamic loads identification based on weighted regularization method," *Journal of Sound and Vibration*, vol. 342, pp. 113–123, 2015.
- [30] C. Cruz and E. Miranda, "Evaluation of the Rayleigh damping model for buildings," *Engineering Structures*, vol. 138, pp. 324–336, 2017.
- [31] Ozkul and T. Aksu, "A finite element formulation for dynamic analysis of shells of general shape by using the Wilson- θ method," *Thin-Walled Structures*, vol. 42, no. 4, pp. 497–513, 2004.
- [32] M. G. Shi, *Science and Engineering Computing Foundation*, Tsinghua University Press, Beijing, China, 1999.
- [33] R. Fletcher, *Practical Methods of Optimization*, Vol. 2, John Wiley and Son's, New York, NY, USA, 2nd edition, 1981.
- [34] L. Wang, X. Zhao, and H. Gao, "A method for determining the regularization parameter and the relative weight ratio of the seismic slip distribution with multi-source data," *Journal of Geodynamics*, vol. 118, pp. 1–10, 2018.
- [35] B. Qiao, X. Zhang, J. Gao, and X. Chen, "Impact-force sparse reconstruction from highly incomplete and inaccurate measurements," *Journal of Sound and Vibration*, vol. 376, pp. 72–94, 2016.
- [36] Y. Hu and Z. Wang, *Finite Element Analysis and Applications*, Tsinghua University Press, Beijing, China, 2009.
- [37] Y. Zhong, "Identification of dynamic parameters for a cantilever beam and design of PD controller," *Automation and Instrumentation*, no. 2, pp. 36–37, 2011.

